© 2018. Published by The Company of Biologists Ltd | Development (2018) 145, dev161018. doi:10.1242/dev.161018

RESEARCH ARTICLE

The DEAD-box RNA helicase Ddx39ab is essential for myocyte and lens development in zebrafish

Linlin Zhang[1,*], Yuxi Yang[1,*], Beibei Li[1], Ian C. Scott[2,3] and Xin Lou[1,‡]

ABSTRACT

RNA helicases from the DEAD-box family are found in almost all organisms and have important roles in RNA metabolism, including RNA synthesis, processing and degradation. The function and mechanism of action of most of these helicases in animal development and human disease remain largely unexplored. In a zebrafish mutagenesis screen to identify genes essential for heart development we identified a mutant that disrupts the gene encoding the RNA helicase DEAD-box 39ab (*ddx39ab*). Homozygous *ddx39ab* mutant embryos exhibit profound cardiac and trunk muscle dystrophy, along with lens abnormalities, caused by abrupt terminal differentiation of cardiomyocyte, myoblast and lens fiber cells. Loss of *ddx39ab* hindered splicing of mRNAs encoding epigenetic regulatory factors, including members of the KMT2 gene family, leading to misregulation of structural gene expression in cardiomyocyte, myoblast and lens fiber cells. Taken together, these results show that Ddx39ab plays an essential role in establishment of the proper epigenetic status during differentiation of multiple cell lineages.

KEY WORDS: RNA helicase, Myocyte, Lens, RNA splicing, Zebrafish

INTRODUCTION

The DEAD-box RNA helicase family is a large group of proteins characterized by the presence of an Asp-Glu-Ala-Asp (DEAD) motif that is highly conserved from bacteria to humans (Bleichert and Baserga, 2007; Rocak and Linder, 2004). Using the energy derived from ATP hydrolysis, these proteins modulate RNA topology and association/dissociation of RNA-protein complexes. DEAD-box RNA helicases play important roles in all aspects of RNA metabolism, including transcription, pre-mRNA splicing, rRNA biogenesis, RNA transport and translation (Calo et al., 2015; Jarmoskaite and Russell, 2011, 2014; Linder and Jankowsky, 2011). Recently, a fuller appreciation of the functions of these RNA helicases in variant physiological or developmental scenarios has started to emerge. Numerous reports have described dysregulation of expression or function of DEAD-box RNA helicases in cancer development or progression, indicating that DEAD-box proteins may be involved in key processes in cellular proliferation (Fuller-Pace, 2013; Sarkar and Ghosh, 2016). Recent reports have further shown that DEAD-box RNA helicases play diverse roles in developmental events ranging from body axis establishment (Meignin and Davis, 2008) to germ cell, blood, digestive organ and brain development (Hirabayashi et al., 2013; Hozumi et al., 2012; Payne et al., 2011; Zhang et al., 2012). These studies indicated that DEAD-box RNA helicase family members can regulate specific developmental processes by affecting pre-mRNA splicing, ribosomal biogenesis or RNA transport.

As a member of the DEAD-box family of ATP-dependent RNA helicases, Ddx39a was originally identified in a screen for proteins that interact with the essential splicing factor U2AF65 (Fleckner et al., 1997). Studies in different organisms indicated that, besides playing an important role in pre-mRNA splicing (Fleckner et al., 1997; Shen et al., 2008, 2007), Ddx39a also acts in mRNA nuclear export (Luo et al., 2001), cytoplasmic mRNA localization (Meignin and Davis, 2008) and maintenance of genome integrity (Yoo and Chung, 2011). However, how Ddx39a functions during embryogenesis, and which RNAs are processed by Ddx39a in different developmental scenarios, remain open to investigation.

In the current study, we examined the function of *ddx39a* in vertebrate development using a newly identified zebrafish *ddx39ab* gene-trap line. Transcriptome profiling and phenotypic analysis of the mutant showed that *ddx39ab* is indispensable for the development of heart, trunk muscle and eyes. Further experiments revealed that Ddx39ab can bind to mRNAs encoding a set of epigenetic regulatory factors, including members of the KMT2 family. Loss of *ddx39ab* results in aberrant pre-mRNA splicing of these epigenetic regulator transcripts, leading to failure in establishment of the proper epigenetic status of multiple structural genes, and eventually hampers the terminal differentiation of cardiomyocyte, myoblast and lens fiber cell lineages.

RESULTS

Loss of *ddx39ab* leads to an embryonic lethal phenotype in zebrafish

In a *Tol2* transposon-mediated gene-trapping screen to identify novel genes involved in cardiovascular system development (Hou et al., 2017), we identified a zebrafish line, RT-011, in which embryos demonstrated a dynamic GFP expression pattern, with strong signal evident in somites and eyes from the 8-somite stage [13 hours post-fertilization (hpf)]. As development proceeded, GFP signal also emerged in the heart (Fig. 1A). Multiple incrosses of RT-011 heterozygotes yielded wild-type, heterozygous, and homozygous mutant embryos at the expected Mendelian ratios, with all homozygous mutant embryos dying by 4 days post-fertilization (dpf). This indicated that the RT-011 trap line carried a recessive lethal allele.

Homozygous mutant embryos from incrosses of heterozygous RT-011 fish showed no obvious morphological defects until 24 hpf (Fig. 1B), at which point contraction of the definitive heart tube was extremely weak and irregular in mutants (Movie 1). Homozygous mutant embryos were completely paralyzed at 24 hpf, and did not

[1]Model Animal Research Center, Nanjing University, Nanjing, 210031, China. [2]Program in Developmental and Stem Cell Biology, The Hospital for Sick Children, Toronto, ON M5G 1X8, Canada. [3]Department of Molecular Genetics, University of Toronto, ON M5S 1A8, Canada.
*These authors contributed equally to this work

‡Author for correspondence (xin.lou@nju.edu.cn)

X.L., 0000-0002-6715-0375

Received 26 October 2017; Accepted 13 March 2018

Development (2018) 145, dev161018. doi:10.1242/dev.161018

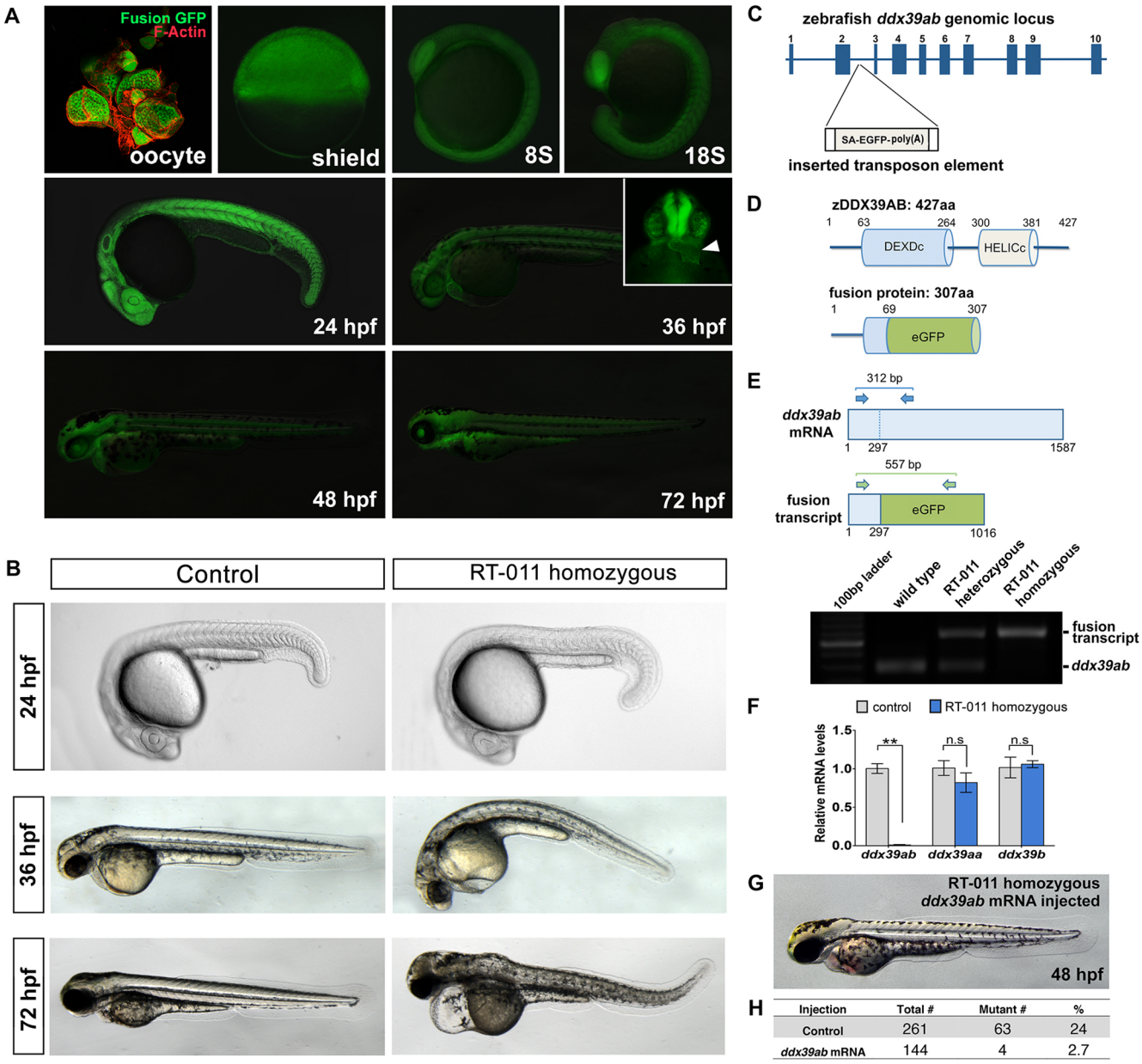

Injection	Total #	Mutant #	%
Control	261	63	24
ddx39ab mRNA	144	4	2.7

Fig. 1. Loss of *ddx39ab* leads to an embryonic lethal phenotype in zebrafish. (A) GFP expression pattern in zebrafish trapping line RP-011. Lateral views. S, somite. Arrowhead in inset indicates GFP expression in heart. (B) Morphological defects in RP-011 homozygous mutant embryos. RP-011 homozygous embryos did not show any morphological defects until 24 hpf; at 48 hpf, they showed a curved body axis, and at 72 hpf heart edema, dysmorphic jaw and widespread degeneration. At least 80 embryos of each genotype were observed and representative samples are shown. (C) The zebrafish *ddx39ab* genomic locus. Exons (blue boxes) are numbered. The transposon is inserted after the second intron. (D) Zebrafish Ddx39ab protein contains DEXDc and HELICc domains. Insertion of the gene-trapping element results in a fusion transcript that will be translated into a fusion protein containing the first 69 amino acids from Ddx39ab at the N-terminus. (E) RT-PCR results showing the presence of fusion transcript in RP-011 embryos. (F) qPCR results showing the absence of *ddx39ab* mRNA in RP-011 homozygous embryos. Data are mean±s.e.m. ***P*<0.01. n.s, not significant. (G) Injection of *ddx39ab* mRNA rescues the developmental defects of RP-011 homozygous embryos. (H) Quantification of the rescue of morphological defects of homozygous *ddx39ab* mutant embryos (Control) by injection of *ddx39ab* mRNA.

exhibit spontaneous tail movements or any response to tactile stimulation (Movie 2). At later stages of development, further defects became apparent, including a failure to establish blood circulation, a curved body axis, prominent cardiac edema, disorganized myotome and extensive cell death (Fig. 1B, Fig. S1).

5′ RACE was used to identify the gene trapped in the RT-011 line. Sequencing indicated that the gene-trapping element was integrated within the second intron of the *ddx39ab* locus (Fig. 1C). Zebrafish Ddx39ab protein contains DEXDc (for ATP binding and hydrolysis) and HELICc (helicase superfamily C-terminal) domains, both of which are highly conserved (over 90% amino acid identity) between zebrafish and human (Fig. S2). The gene-trap insertion resulted in a transcript that encodes a fusion protein containing the first N-terminal 69 amino acids of Ddx39ab (Fig. 1D). Since this fusion protein lacked both the DEXDc and HELICc domains, the allele that we identified from the RT-011 line should act as a true null allele. RT-PCR analysis clearly showed the presence of the *ddx39ab-GFP* fusion transcript in heterozygous

Development (2018) 145, dev161018. doi:10.1242/dev.161018

RT-011 embryos and the absence of wild-type *ddx39ab* transcript in homozygous embryos (Fig. 1E).

To confirm that mutation of *ddx39ab* represents the causal event in the homozygous RT-011 phenotype, the expression level of *ddx39ab*, *ddx39aa* and *ddx39b* was examined, and only expression of *ddx39ab* was found to be absent in homozygous gene-trap embryos (Fig. 1F). Furthermore, when mRNA encoding wild-type Ddx39ab was injected into embryos from incrosses of heterozygous RT-011 fish, the morphological defects of the homozygous RT-011 embryos were efficiently rescued (Fig. 1G,H), with injected mutant embryos surviving up to 9 dpf. Taken together, these findings indicated that the developmental abnormalities of RT-011 homozygous embryos result from mutation of *ddx39ab*.

To further confirm the endogenous embryonic expression of *ddx39ab*, whole-mount RNA *in situ* hybridization was carried out on wild-type embryos. *ddx39ab* was strongly expressed during early embryogenesis, with abundant transcript localized to the myotome, heart and eyes. As development proceeded, *ddx39ab* expression became restricted to several tissues, including the pharyngeal arches and liver (Fig. S3). The dynamic expression pattern of *ddx39ab* indicated possible roles in multiple developmental stages and tissues.

Developmental defects in muscular organs and lens in *ddx39ab* mutants

Based on the expression pattern during embryogenesis and defects displayed in *ddx39ab* homozygous mutants, we examined development of the heart, skeletal muscle and lens in *ddx39ab* mutant embryos.

At 36 hpf, the heart tube in wild-type embryos had undergone looping and chamber ballooning, becoming a functional two-chamber pump. By contrast, hearts of *ddx39ab* mutants were morphologically abnormal, with little looping or chamber emergence evident (Fig. 2A, left). Immunostaining revealed that the cardiac sarcomere was severely disorganized in *ddx39ab* mutants as compared with control embryos (Fig. 2A, middle and right).

Gene expression analysis of a number of cardiac markers at 26 hpf demonstrated that loss of *ddx39ab* did not cause a readily apparent decrease in the expression of many cardiogenic regulatory genes, including *nkx2.5*, *gata5*, *tbx5a* and *bmp4* (Fig. 2B; data not shown). Specification of both heart chambers occurred properly in *ddx39ab* mutants, as shown by expression of *myh6* and *myh7* (Fig. 2C). By contrast, *ddx39ab* mutant embryos demonstrated significantly reduced expression of *nppa*, a gene associated with maturation of the heart tube (Auman et al., 2007). Expression of a number of cardiac sarcomere structural genes was also distinctly downregulated in *ddx39ab* mutant embryos, including *myh6*, *cmlc1*, *acta1b* and *ttn.2* (Fig. 2C). Decreased expression of these cardiac sarcomere components might represent the causal factor for the weak contractility observed in *ddx39ab* mutant hearts.

Next, we examined whether the locomotion defect in *ddx39ab* mutant embryos reflected altered skeletal muscle organization. Immunohistochemical staining for myosin heavy chain (MF20 antibody) and F-actin revealed that myofibrillar protein assembly was severely disrupted in *ddx39ab* mutant embryos when compared with wild type (Fig. 3A). To determine which step of muscle development was affected, *ddx39ab* mutant embryos were analyzed for myoblast differentiation by RNA *in situ* hybridization for genes encoding myogenic regulatory factors (Bentzinger et al., 2012). The expression of early myogenic specification markers (*myod1* and *myf5*) and late differentiation markers (*myogenin* and *myf6*) appeared normal until 32 hpf (Fig. 3B; data not shown). Similar to the myocardium, the expression of a battery of sarcomeric components, including *tnnt2d*, *myhz2* and *smyhc1*, was significantly reduced in the *ddx39ab* mutant embryos at 32 hpf (Fig. 3C,D). This indicated that maturation of both fast muscle and slow muscle was compromised in *ddx39ab* mutants. We also found reduction in transcript levels of *casq1a*, which encodes a calcium-binding protein of the skeletal muscle sarcoplasmic reticulum (Yazaki et al., 1990), and *slc25a4*, which encodes a muscle cell-specific mitochondrial ATP-ADP carrier (Gutiérrez-Aguilar and Baines, 2013) (Fig. 3C). These results suggested that *ddx39ab* plays an important role in skeletal muscle maturation and function.

As *ddx39ab* demonstrated strong expression in developing eyes, we next examined the development of retina and lens in *ddx39ab* mutants. Sectioning of retinas at 32 hpf revealed that pigmented epithelium formed and retinal neuroepithelium displayed normal histological features in *ddx3ab* mutants. Further analysis revealed that retinal neuron production (marked by *atoh7* expression) and ganglion cell differentiation (marked by *lhx3* and Alcama expression) were initiated normally in *ddx39ab* mutant retina (Fig. S4). These data indicated that development of the retina was largely normal. At 28 hpf, the lens of *ddx39ab* mutant embryos displayed no obvious defects at the level of gross morphology, with cell number being comparable in *ddx39ab* mutant and wild-type embryos (Fig. 4A).

During eye morphogenesis, cells in the center of the lens mass retain spheroidal morphology, differentiating as primary fibers (which originate from the central lens placode) that elongate and wrap around the ovoid-shaped cells in the center, resulting in crescent-shaped layers of fibers (Greiling and Clark, 2009). In contrast to wild type, in *ddx39ab* mutants a majority of lens fiber cells did not form crescent-shaped layers, instead showing a relatively irregular and convex shape with significantly higher convexity (Fig. 4A, bottom; Fig. S5). We next analyzed the expression of lens-specific genes in order to explore the nature of the disorganization of primary fiber cells in *ddx39ab* mutant embryos. We first examined the expression of a cascade of upstream transcription factors that drive fiber cell differentiation, including *prox1a*, *foxe3* and *pitx3* (Cvekl and Duncan, 2007; Greiling and Clark, 2012; Pillai-Kastoori et al., 2015). In *ddx39ab* mutants, the transcription of *foxe3* was mildly upregulated, whereas no overt changes in *pitx3* and *prox1a* expression were observed (Fig. 4B). During lens fiber cell elongation, soluble proteins known as crystallins are abundantly expressed in lens fibers to increase the refractive index and contribute to transparency (Clark, 2004). We found that the expression of crystallin genes, including *cryaa*, *crygm2d10* and *crygm2d1*, was dramatically downregulated in *ddx39ab* mutant embryos (Fig. 4C). Differentiated lens fiber cells express a set of cell-cell adhesion molecules required for refractive index matching of lens membranes and cytoplasm (Bassnett et al., 2011). *In situ* hybridization and qPCR demonstrated that in *ddx39ab* mutant embryos the expression of *lim2.4*, a lens-specific receptor for Calmodulin involved in cell junction organization, was notably downregulated (Fig. 4C). Bfsp1 (also known as Filensin) and Bfsp2 (also known as Phakinin) are assembly partners of the beaded-chain filament, a type of lens-specific cytoskeletal element. Significant downregulation of these two genes in *ddx39ab* mutant lens was also observed (Fig. 4C). These data indicated that *ddx39ab* is also indispensable for lens fiber cell terminal differentiation.

The above results indicated that *ddx39ab* deletion causes dysregulated expression of structural genes during terminal differentiation of cardiomyocyte, myocyte and lens fiber cells. This hampered cell differentiation in turn leads to multiple defects in

Development (2018) 145, dev161018. doi:10.1242/dev.161018

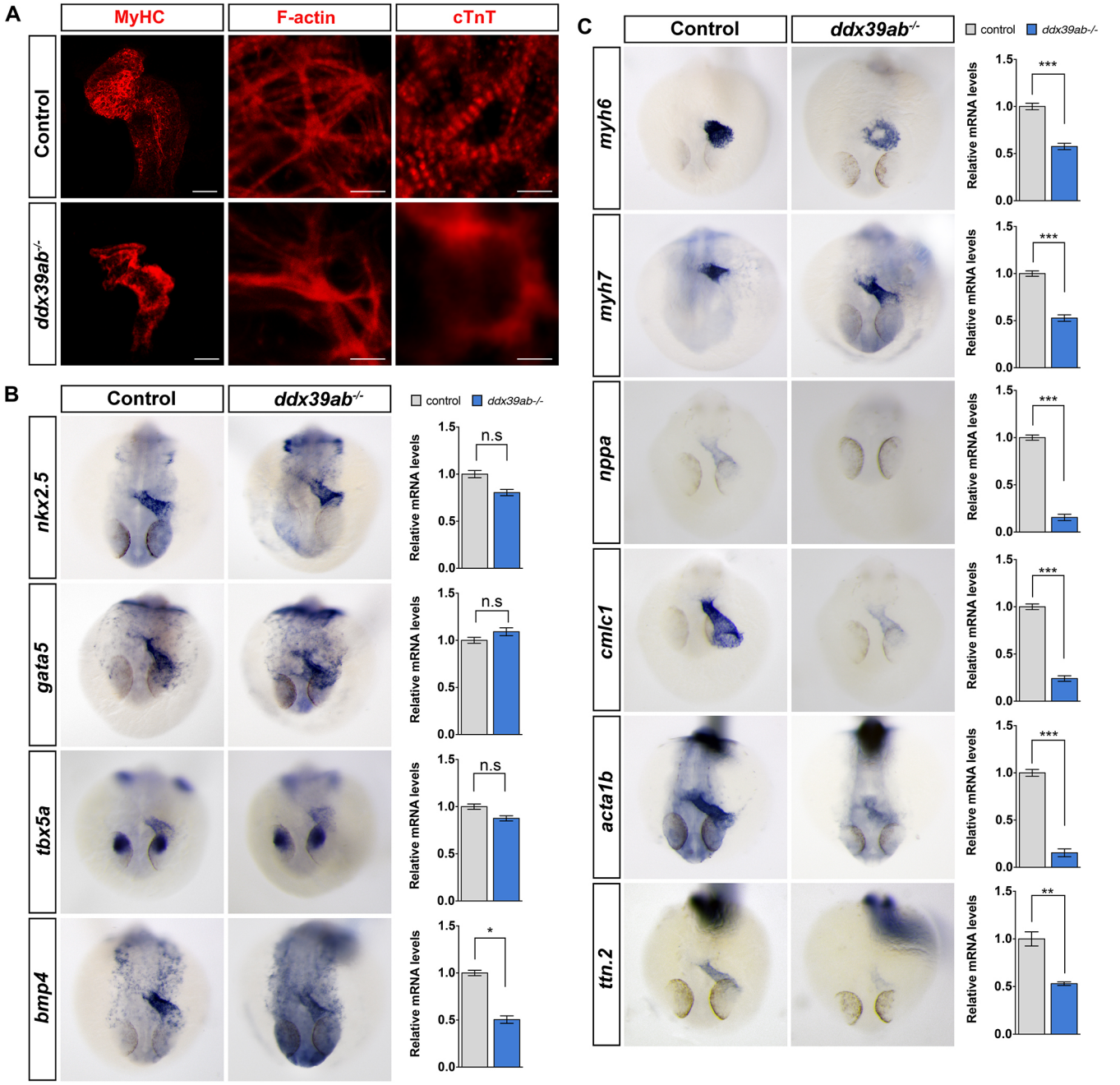

Fig. 2. Loss of *ddx39ab* leads to cardiomyocyte differentiation defects in zebrafish embryos. (A) Ventral view of heart from whole-mount wild-type or *ddx39ab* mutant zebrafish embryos at 36 hpf, with cranial to the top. Myocardium was labeled with MF20 antibody. Scale bars: 200 µm. (B) RNA *in situ* hybridization and qPCR results for cardiogenic regulatory gene expression in wild-type and *ddx39ab* mutant zebrafish embryos at 26 hpf. (C) RNA *in situ* hybridization and qPCR results for cardiomyocyte structural gene expression in wild-type and *ddx39ab* mutant zebrafish embryos at 26 hpf. (B,C) Frontal views with dorsal side to the top. At least 15 (A) or 20 (B,C) embryos for each genotype were analyzed and representative samples are shown. For qPCR results, data are mean±s.e.m. n.s, not significant. **P*<0.05, ***P*<0.01, ****P*<0.001.

the muscular organs and eyes that are likely to contribute collectively to the lethal phenotype of *ddx39ab* mutant zebrafish embryos.

Changes in the transcriptomic landscape in *ddx39ab* mutants

DEAD-box RNA helicases regulate multiple facets of RNA metabolism (Linder and Jankowsky, 2011). In order to determine how mutation of *ddx39ab* affects the zebrafish embryo transcriptome, we performed RNA-seq on wild-type and *ddx39ab* mutant embryos at 24 hpf. A total of 878 genes, consisting of 548 with decreased and 330 with increased expression, were significantly altered in the *ddx39ab* mutant embryos [fold change (FC)>2, false discovery rate (FDR)<0.05] (Fig. 5A; Table S3). Following gene ontology (GO) analysis, we found that genes downregulated in *ddx39ab* mutants were enriched for GO terms linked to development of muscular tissue and lens (Fig. 5B). Interestingly, consistent with previous observations revealed by *in situ* hybridization, in all three cell types (cardiomyocyte, myocyte and lens fiber cells), the expression of upstream regulatory factors

Development (2018) 145, dev161018. doi:10.1242/dev.161018

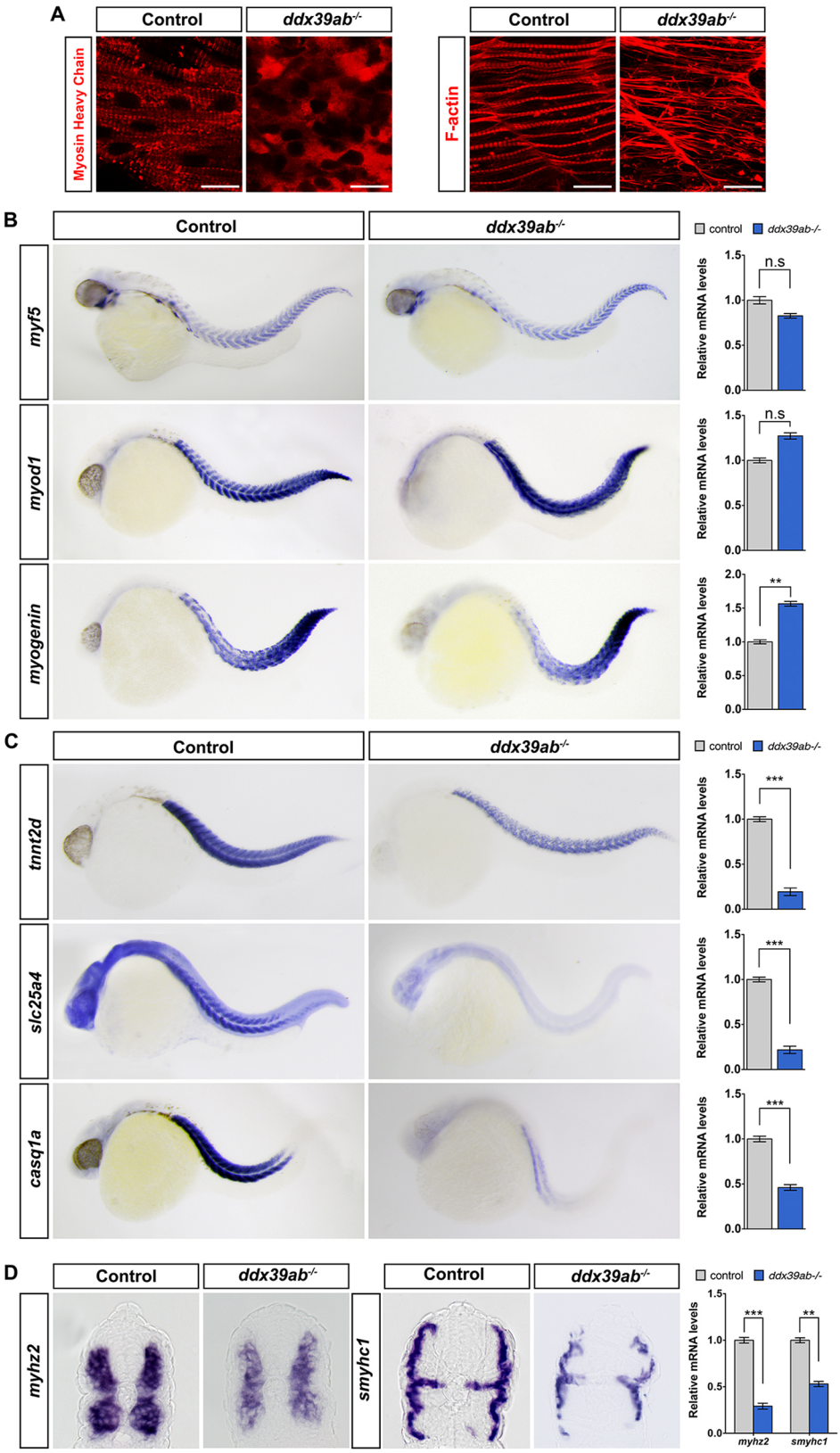

Fig. 3. Loss of *ddx39ab* results in defective skeletal muscle differentiation in zebrafish. (A) Immunostaining demonstrates the organization of myofilaments in wild-type and *ddx39ab* mutant embryos at 24 hpf. Anti-MHC antibody (MF20) labels thick (myosin) filaments and F-actin was visualized by phalloidin staining. Scale bars: 20 µm. (B) RNA *in situ* hybridization for myogenic regulatory gene expression in wild-type and *ddx39ab* mutant zebrafish embryos at 32 hpf. (C,D) RNA *in situ* hybridization and qPCR analysis for myocyte structural gene expression in wild-type and *ddx39ab* mutant zebrafish embryos at 32 hpf. (B,C) Lateral views with anterior to the left. (D) Transverse section with dorsal side to top. At least 15 (A) or 20 (B-D) embryos of each genotype were analyzed and representative samples are shown. For qPCR results, data are mean±s.e.m. n.s, not significant. ***P*<0.01, ****P*<0.001.

Development (2018) 145, dev161018. doi:10.1242/dev.161018

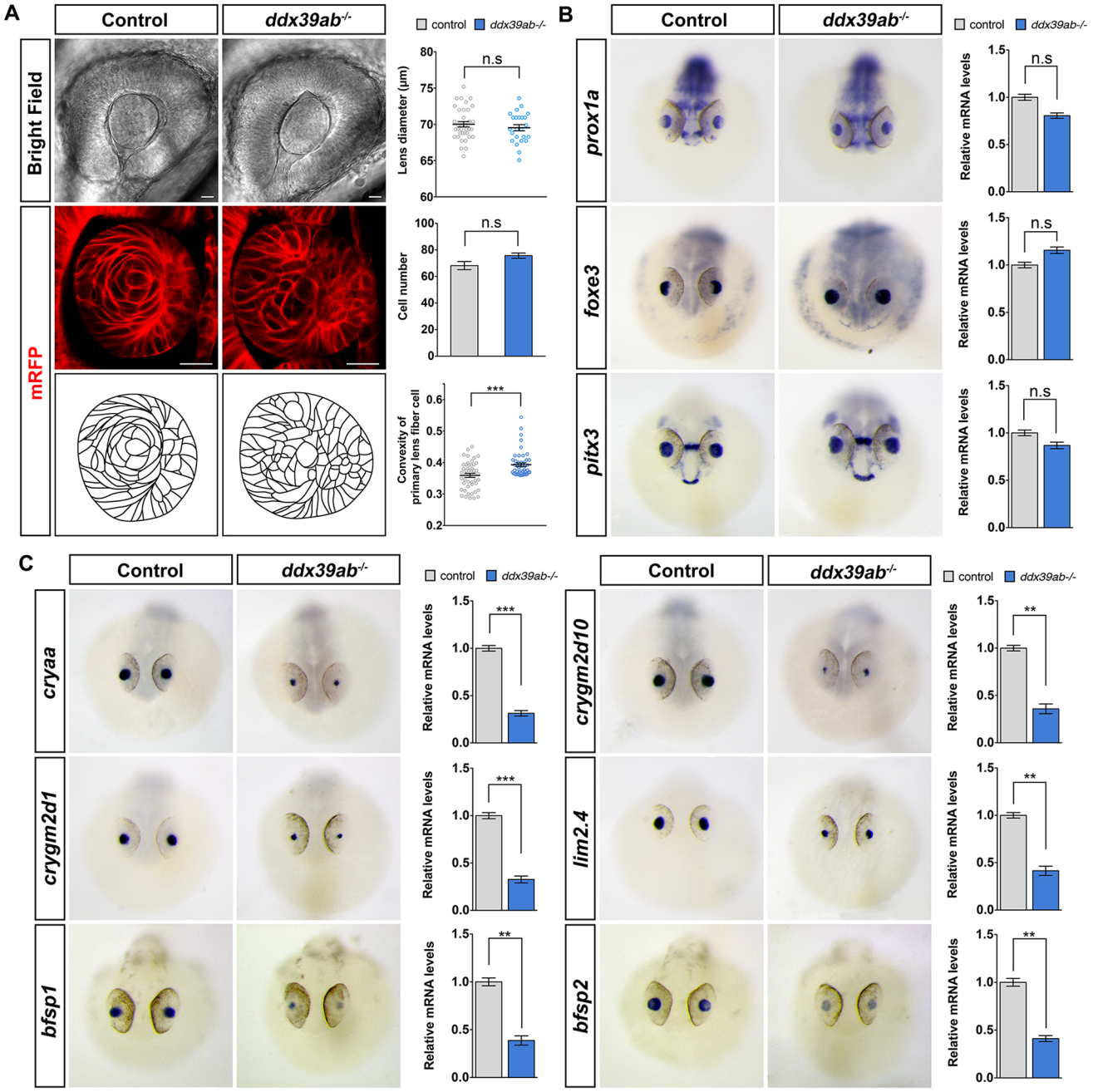

Fig. 4. Lens fiber cell differentiation is defective in *ddx39ab* mutant embryos. (A) *ddx39ab* mutants exhibit defects in lens fiber morphogenesis. (Top) Bright-field images of the eyes from wild-type and *ddx39ab* mutant zebrafish embryos at 28 hpf. The scatter plot shows the diameter of individual lens fibers. (Middle) Equatorial sections through the lens center showing the organization of lens fibers; cell membrane is labeled with mRFP. Cell number was quantified on equatorial sections. (Bottom) Schematics showing the shape and arrangement of lens fiber cells. The convexity of lens fiber cells is plotted. Scale bars: 50 μm. (B,C) RNA *in situ* hybridization and qPCR results for lens gene expression in wild-type and *ddx39ab* mutant zebrafish embryos at 32 hpf. Frontal views with dorsal side to the top. (A-C) At least 20 embryos of each genotype were analyzed and representative samples are shown. All data are mean±s.e.m. n.s, not significant. ***P*<0.01, ****P*<0.001.

showed no evidence of change, whereas the expression of many structural constituents was greatly diminished (highlighted in Fig. 5B). These results further suggested that *ddx39ab* plays a common and important role in the terminal differentiation of cardiomyocyte, myocyte and lens fiber cells.

To gain further insight into the impact on transcript levels caused by loss of *ddx39ab*, we examined alternative splicing using the OLego program and the Quantas pipeline. 12,236 significant alternative splicing events (|dI|>0.1; Table S4) were scored in *ddx39ab* mutant embryos compared with controls. These events include skipping/inclusion of single or tandem cassette exons, intron retention and the use of alternative 5′ or 3′ splice sites (Table S4; number of events shown in Fig. 5C). These data showed that loss of Ddx39ab leads to extensive intron retention events and cassette skipping, implicating Ddx39ab functions in intron definition. The mixed splicing activities (skipping and inclusion) observed in *ddx39ab* mutants clearly suggest that context-dependent splicing defects result from the loss of Ddx39ab.

Development (2018) 145, dev161018. doi:10.1242/dev.161018

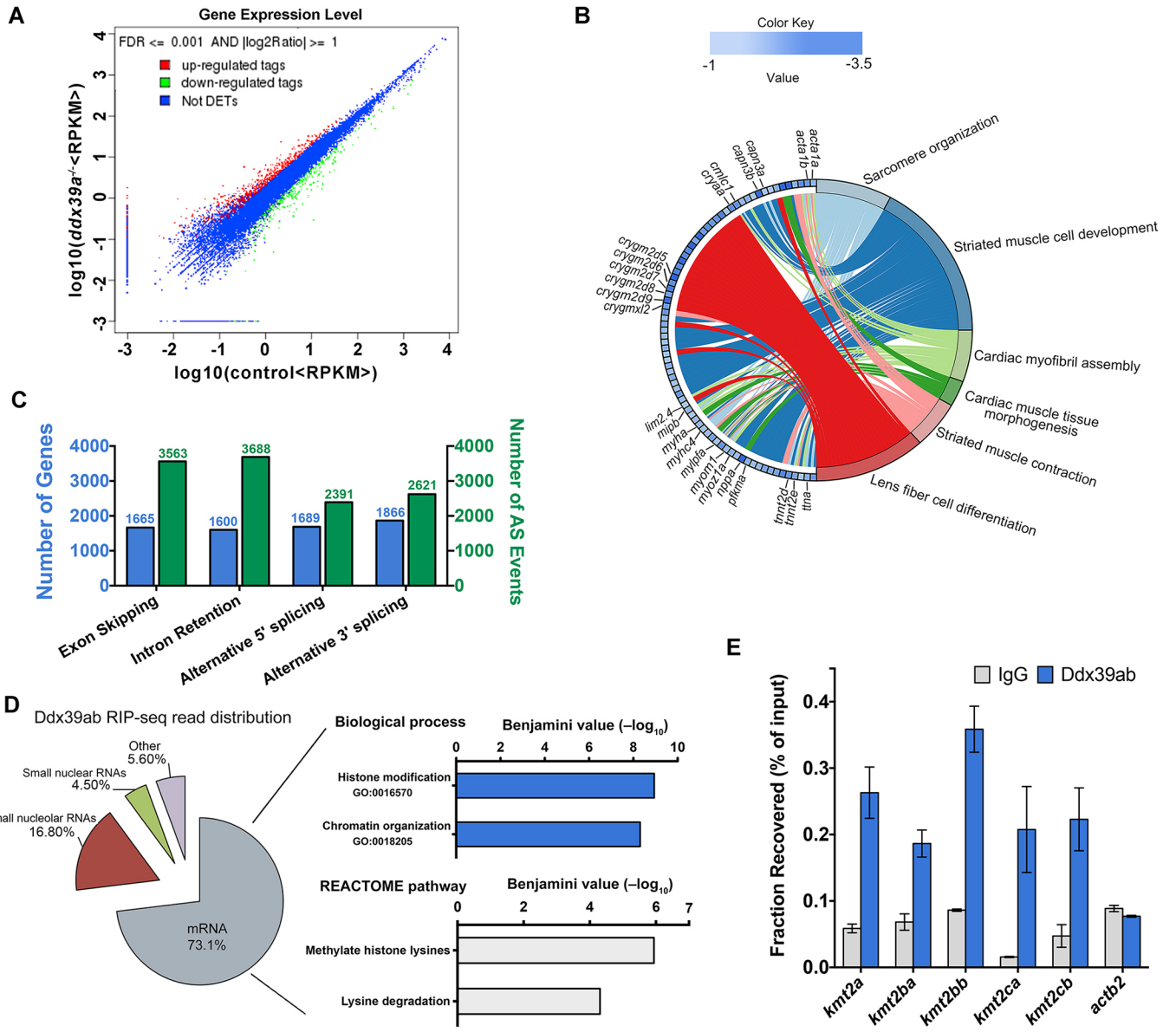

Fig. 5. Transcriptome landscape of *ddx39ab* mutants and identification of Ddx39ab-associating RNAs. (A) Expression levels of differentially expressed genes in control and *ddx39ab* mutant embryos. Upregulated and downregulated genes are denoted by red and green spots, respectively, while genes that were not differentially expressed (Not DETs) are denoted by blue spots. RPKM, reads per kilobase per million mapped reads. (B) Circular plot showing 77 representative downregulated genes belonging to enriched functional categories, simultaneously presenting a detailed view of the relationships between expression changes (left semicircle perimeter) and GO (right semicircle perimeter). Complete gene lists and GO term tables are presented in Table S5. (C) Distribution of various alternative splicing (AS) events in *ddx39ab* mutant embryos. Details are provided in Table S4. (D) (Left) Ddx39ab RIP-seq reads annotated to the zebrafish genome, with percentage of total RIP-seq reads shown. (Right) Enriched GO and REACTOME pathway terms from Ddx39ab-bound mRNAs obtained using DAVID. The *x*-axis values correspond to the negative Benjamini *P*-value. (E) RIP-qPCR showing binding of Ddx39ab to selected epigenetic modulator genes. Mean±s.e.m. *actb2* was included as negative control.

ddx39ab deletion affects pre-mRNA splicing of KMT2 family genes

We proposed that defining the RNA interactome of Ddx39ab would reveal insights into the molecular mechanisms underlying the phenotypes of *ddx39ab* mutant embryos. To systematically identify Ddx39ab-associated RNAs, RNA immunoprecipitation sequencing (RIP-seq) was performed in *ddx39ab* mutant embryos injected with mRNA encoding Flag-tagged Ddx39ab (Flag-Ddx39ab). Sequencing results showed that Ddx39ab interacts with a diverse set of RNAs (Table S6), of which mRNAs were highly represented (73.1%), with snoRNAs and rRNA contributing 16.8% and 4.5%, respectively, of bound transcripts (Fig. 5D). Comparison of data from RIP-seq and RNA-seq revealed that 84% of Ddx39ab-associated mRNAs showed alternative splicing in *ddx39ab* mutants (which we refer to as high-confidence Ddx39ab target transcripts), underscoring the function of Ddx39ab in pre-mRNA splicing. GO term and pathway analysis linked these Ddx39ab-associating mRNAs to histone modification. Among these potential Ddx39ab target mRNAs, members of the KMT2 gene family (*kmt2a*, *kmt2ba*, *kmt2bb*, *kmt2ca* and *kmt2cb*) were prominent. KMT2 family members methylate lysine 4 on the histone H3 tail, a crucial regulatory step in myogenesis associated with the modulation of chromatin structure and DNA accessibility (Lee et al., 2013; Rao and Dou, 2015).

Development (2018) 145, dev161018. doi:10.1242/dev.161018

To confirm interactions between Ddx39ab and KMT2 family member mRNAs, RNA immunoprecipitation and quantitative reverse-transcription PCR (RIP-qPCR) was applied. This further verified that Ddx39ab could bind to these mRNAs (Fig. 5E). We examined splicing events of KMT2 family genes in control and *ddx39ab* mutant embryos by RT-PCR analysis (Ríos et al., 2011; Rösel et al., 2011). This showed that unspliced mRNAs were retained at higher levels in *ddx39ab* mutants versus controls at 24 hpf (Fig. 6A), suggesting that the pre-mRNA splicing of these genes was defective. As a control, we confirmed that in *ddx39ab* mutants the splicing of the housekeeping gene *actb1* was normal. These results suggest that in *ddx39ab* mutants the effect on pre-mRNA splicing might be specific to a certain set of genes.

KMT2s are the major histone methyltransferases responsible for mono-methylation at lysine 4 of histone H3 (H3K4me1) at distal enhancers and regions flanking the transcription start site (TSS) (Rao and Dou, 2015). To investigate whether loss of *ddx39ab* affects the presence of H3K4me1 on actively transcribed genes, ChIP-qPCR was performed for a selected set of genes that showed altered transcript levels in *ddx39ab* mutant versus control embryos at 24 hpf. Whereas global H3K4me1 levels in *ddx39ab* mutants showed only minor decreases compared with wild type (Fig. S6), the H3K4me1 occupancy at regions flanking the TSS of myocyte- and cardiomyocyte-specific genes (*acta1b*, *myhz2*, *nppa*, *myom1a*, *tnnt2d*, *mylpfb* and *smhyc1*) was significantly reduced in the mutants (Fig. 6B). Interestingly, the H3K4me1 occupancy level in the TSS region of myogenic regulatory factors (such as *myod1*) was comparable in control and *ddx39ab* mutant embryos, consistent with the analysis of transcript and protein levels by RNA-seq, *in situ* hybridization and western blot (Fig. 6B, Fig. S6).

These results support a context-dependent requirement of Ddx39ab for proper pre-mRNA splicing of KMT2 family members, with loss of *ddx39ab* leading to failure in establishment of the epigenetic status required for terminal differentiation.

DISCUSSION

Members of the DEAD-box RNA helicase family have been shown to be involved in nearly all aspects of RNA metabolism, from transcription to mRNA decay. Recent studies have started to delineate different functions of DEAD-box RNA helicases in a broader context, including animal development. For example, *ddx46* is expressed in the digestive organs and brain and has been shown to be required for the development of these organs (Hozumi et al., 2012). Researchers have also reported that *ddx18* is essential for hematopoiesis (Payne et al., 2011). The generation of the *ddx39ab* gene-trapping allele provided the opportunity to study the function of this gene in vertebrate development. Here we demonstrated that *ddx39ab* is required for normal gene expression and differentiation of cardiomyocyte, myocyte and lens fiber cells. In previous studies, the development and function of the heart was shown to be sensitive to defects in RNA metabolism (Ding et al., 2004; Xu et al., 2005). Our observations corroborate these results and suggest that myocyte and lens fiber differentiation similarly bear this cell type-specific susceptibility. One possible explanation for this observation is that these three cell types exploit a similar, KMT2 family-dependent mechanism to establish epigenetic status during differentiation. An alternative hypothesis is that, compared with other cell types (such as neurons), a larger fraction of splicing undergoes Ddx39ab-related regulation in these three types of cell. FACS followed by RIP-seq might identify cell type-specific Ddx39ab-associated transcripts, and this information might help to clarify the underlying mechanisms of cell type-specific susceptibility.

RNA-binding proteins (RBPs) including DEAD-box RNA helicases modulate splicing primarily by positively or negatively regulating splice site recognition by the spliceosome. Recognition by RBPs relies on distinct regulatory sequences in pre-mRNAs that function as splicing enhancers or silencers. Our data showed that Ddx39ab can bind to a battery of mRNAs, although more sophisticated molecular biology and bioinformatics efforts need to be exploited to unfold the detailed mechanism of Ddx39ab-mediated splicing events, such as how the specificity is defined.

During development, *ddx39ab* shows a complex and dynamic expression pattern (Fig. 1, Fig. S3). This prompts future analysis of the role of *ddx39ab* in later developmental events (e.g. during formation of the pharyngeal arches and the development of digestive organs). However, the severe defects observed in *ddx39ab* mutants at early stages of development complicates the analysis of later developmental events. CRIPSR/Cas9-based generation of tissue-specific *ddx39ab* mutants, or generation of a conditional *ddx39ab* allele, will be required to study *ddx39ab* function in other organs/tissues.

Previous studies showed that Ddx39ab acts as a growth-associated factor in cancer cells that is required for genome integrity and telomere protection (Sugiura et al., 2007; Yoo and Chung, 2011). We did not detect abnormal mitoses in *ddx39ab* mutant embryos (Fig. S7). However, analysis of later stage *ddx39ab* mutants might be required to observe telomeric defects, after a sufficient number of cell divisions have occurred. It might also be the case that the telomere protection function of Ddx39ab is not conserved between fish and mammals.

It was interesting to note that among a relatively small number of genes significantly downregulated in *ddx39ab* mutant embryos, a large proportion of them encoded structural constituents, including sarcomeric components in muscle cells and crystallin genes in lens fiber cells. In addition to regulating mRNA splicing, it is possible that Ddx39ab is involved in transactivation of structural components via an uncharacterized mechanism that is exploited in both muscular and lens fiber cells. Several studies have shown that DEAD-box proteins play important roles as regulators of transcription, particularly as co-activators or co-suppressors of transcription (Fuller-Pace and Nicol, 2012; Huang et al., 2015). Further investigation to determine which proteins Ddx39ab directly binds to in various cell types, and the functional consequences of these interactions, should provide important insight into how the specificity of Ddx39ab function is regulated.

MATERIALS AND METHODS

Ethics approval

Zebrafish were maintained and handled in accordance with approved guidelines of the Institutional Animal Care and Use Committee of Nanjing University and as per Canadian Council on Animal Care and Hospital for Sick Children Laboratory Animal Services guidelines.

Zebrafish lines

Zebrafish embryos were maintained and staged using standard techniques (Westerfield, 1993). The RP-T gene-trap vector was modified from RP2 (Clark et al., 2011) by switching the monomeric RFP to monomeric GFP. RP-T plasmid (25 ng/µl) and Tol2 transposase mRNA (50 ng/µl) were injected (1 nl each) into 1-cell stage embryos as described (Hou et al., 2017). To identify the affected gene in the gene-trap lines, inverse PCR and 5′ RACE were performed as described (Clark et al., 2011). The gene-trapping

Development (2018) 145, dev161018. doi:10.1242/dev.161018

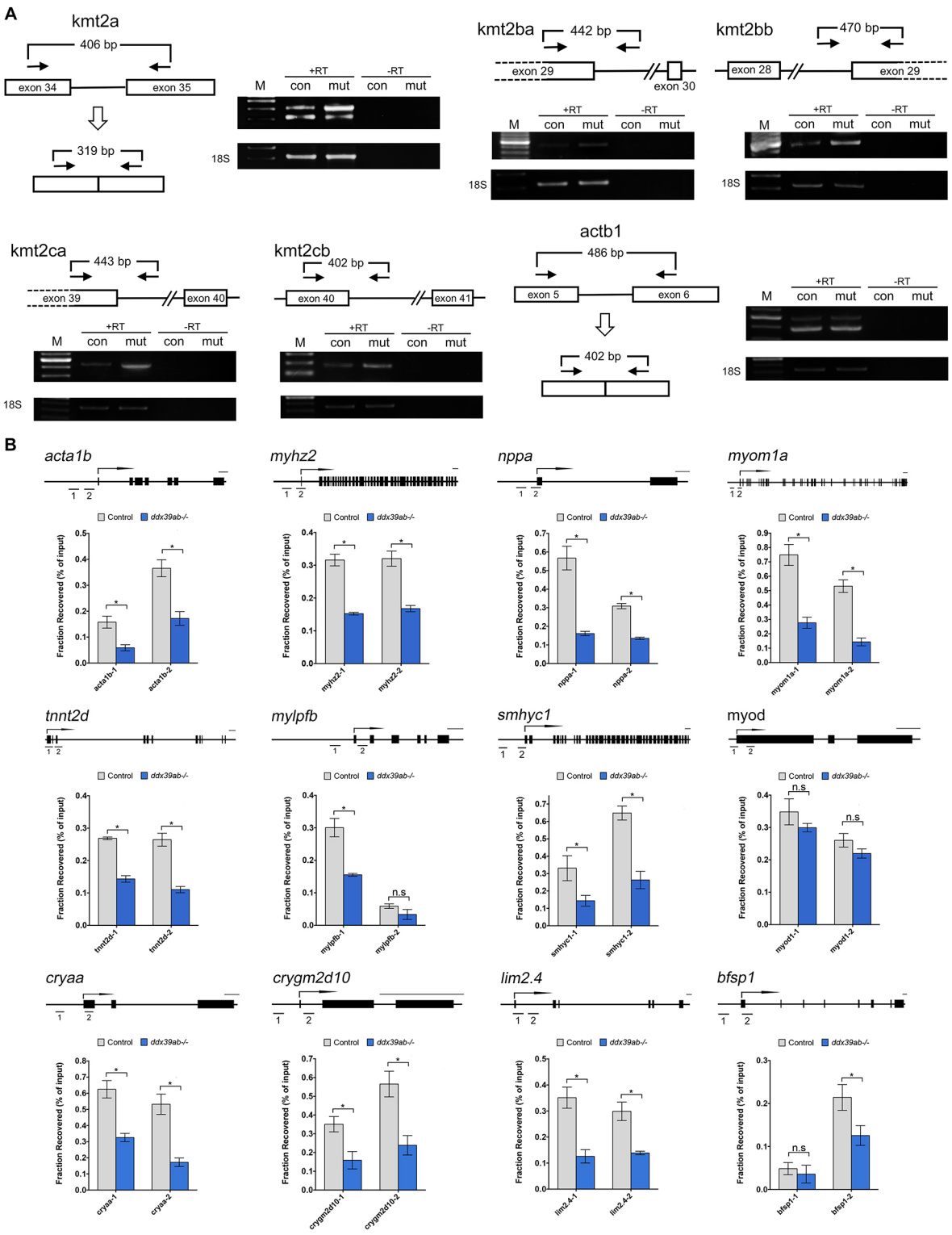

Fig. 6. *ddx39ab* deficiency affects pre-mRNA splicing of epigenetic modulator genes. (A) The splicing status of *kmt2a*, *kmt2ba*, *kmt2bb*, *kmt2ca*, *kmt2cb* and *actb1* pre-mRNA was monitored by RT-PCR with the primers illustrated (arrows). Boxes, exons; lines, introns. Unspliced *kmt2a*, *kmt2ba*, *kmt2bb*, *kmt2ca* and *kmt2cb* mRNAs were retained in the *ddx39ab* mutant (mut) compared with control (con) larvae. Unspliced and spliced PCR products were verified by sequencing. –RT, control without reverse transcriptase. 18S is a loading control. M, DNA size markers. Control larvae were sibling wild-type or *ddx39ab* heterozygous larvae and had normal phenotypes. (B) ChIP-qPCR analyses showing the effect of loss of *ddx39ab* on H3K4 methylation levels at the promoter and TSS of muscle cell and lens fiber cell genes. Gene structure is shown above (rectangles, exons; arrow, TSS) with the DNA segments amplified by PCR indicated. *n*=3. Results are mean±s.e.m. n.s, not significant. **P*<0.05.

insertion position in the *ddx39ab* locus was determined by sequencing. For PCR genotyping of single embryos, primers were designed to differentially amplify the wild-type allele or gene-trap allele. After immunostaining or *in situ* hybridization, genotyping PCR was applied as previously described (Kawakami et al., 2016). Primer pairs and detailed PCR conditions for genotyping are listed in Table S1.

Development (2018) 145, dev161018. doi:10.1242/dev.161018

Reverse-transcription PCR (RT-PCR)

Total RNA was prepared using TRIzol (Invitrogen, Life Technologies), with DNase-treated RNA reverse transcribed using random 16-mer priming and SuperScript II reverse transcriptase (Life Technologies). PCR was performed with primers specifically amplifying cDNA from *ddx39ab* mRNA or fusion transcript. Primer pairs and detailed PCR conditions are listed in Table S1.

Quantitative RT-PCR (RT-qPCR)

Embryos from three different clutches were collected as biological replicates and total RNA was prepared using TRIzol. RNA was reverse transcribed with a mix of oligo(dT) and random 16-mer priming and SuperScript II reverse transcriptase. Quantitative PCR (qPCR) assays were performed in triplicate with SYBR Green Master Mix (Takara) according to the manufacturer's instructions. Melting curves were examined to ensure primer specificity. Results were analyzed using the standard ΔΔCT method (Schmittgen and Livak, 2008). 18S rRNA served as the reference gene in all analyses, and changes in mRNA levels relative to 18S rRNA were confirmed using *actb2* as an alternate reference gene in independent experiments. Primers used for qPCR analysis are listed in Table S1.

Statistics

Two-sided, paired Student's *t*-tests were applied for RT-qPCR and ChIP-qPCR results; two-sided, unpaired Student's *t*-tests were applied for other quantification experiments. Significance of differences was calculated with GraphPad Prism6. $P<0.05$ was considered significant.

mRNA injections

pCS2+ vectors carrying a cDNA fragment encoding membrane RFP (mRFP), Ddx39ab, Flag-Ddx39ab and Tol2 transposase were used. Capped mRNA was synthesized using the SP6 mMESSAGE mMACHINE Kit (Ambion, Life Technologies). For phenotype rescue experiments, *ddx39ab* mRNA (100 pg) was injected at the 1-cell stage.

Immunocytochemistry

Embryos were fixed in 4% paraformaldehyde at 4°C overnight. Embryos were blocked with blocking solution (1× PBS, 1% BSA, 1% Triton X-100, 0.1% DMSO) for 2 h then incubated with primary antibodies diluted in blocking solution overnight at 4°C. Embryos were washed three times in 1× PBS with 1% Triton X-100 for 15 min each. Embryos were incubated with secondary antibodies diluted in blocking solution for 2 h. Primary antibodies specific to Myh1a, Myh1e, Cardiac troponin T (cTnT; Tnnt2), and acetylated Tubulin were used. Fluorescent immunocytochemistry was performed using anti-mouse antibody conjugated with actin filaments, as visualized with Rhodamine-conjugated phalloidin. Unless otherwise stated, manipulations were performed at room temperature. Detailed information on antibodies and dilutions is provided in Table S2.

Imaging

Embryo whole-mount imaging was performed using a Leica DFC320 camera on a Leica M205FA stereomicroscope. Confocal images were taken using a Zeiss LSM880 confocal microscope.

RNA *in situ* hybridization

RNA *in situ* hybridization using DIG-labeled antisense RNA probes was carried out as previously described (Thisse and Thisse, 2008).

Western blotting

Western blotting analysis of myocyte or cardiomyocyte transcriptional regulators and H3K4Me1 in control and *ddx39ab* mutant embryos at different stages was performed as described in the supplementary Materials and Methods using the primary antibodies listed in Table S2.

Characterization of lens defects

To quantify lens equatorial width, bright-field images from live embryos were taken with a Nikon ECLIPSE Ni microscope and measured with the Nikon Elements BR measurement tool. At least 20 embryos of each genotype were measured under identical conditions. To quantify the number and convexity of lens fiber cells, mRFP mRNA was injected into embryos at the 1-cell stage and at 28 hpf, and confocal images for equatorial sections from control and *ddx39ab* mutant embryos were taken. Cell numbers on optical sections were counted manually. Cell convexity was calculated with the 3D Convex Hull plug-in of ImageJ (Sheets et al., 2011). Convexity was defined as the ratio between convex surface area and total surface area.

RNA-seq for expression and splicing analysis

Total RNA from 100 control and *ddx39ab* mutant 24 hpf embryos was isolated using TRIzol reagent. Two biological replicates for each group (control and *ddx39ab* mutant) were processed and sequenced. Sequencing libraries were prepared using the Nextera sample preparation kit (Illumina) and subjected to HiSeq paired-end 100 bp plus sequencing. Resulting reads were aligned to the zebrafish reference genome (GRCz10) and gene expression quantified using TopHat V2.2.1 and Bowtie2 v2.2.3 (Kim et al., 2013; Langmead and Salzberg, 2012). Differential gene expression was analyzed using HTSeq v0.6.1p1 (Anders et al., 2015). Genes showing altered expression with adjusted $P<0.05$ were considered differentially expressed. For the set of differentially expressed genes a functional analysis was performed using Ingenuity Pathway Analysis software and DAVID (Huang et al., 2009), and some of the enriched processes were selected according to relevant criteria related to the biological process studied. Using the R visualization package GOPlot (Walter et al., 2015), a chord plot was generated to better visualize the relationships between genes and the selected enriched processes. OLego (Wu et al., 2013) and Quantas pipelines were used for alternative splicing analysis. Transcript structure was inferred between paired-end reads. Alternative splicing was quantified by separating genomic and junction reads and scoring the output from transcript inference. Finally, statistical tests were run to filter the significant alternative splicing events (Fisher's exact test and Benjamini FDR).

RNA immunoprecipitation and RIP-seq

RNA immunoprecipitation (RIP) was performed as previously described (Jain et al., 2011) with the specific modifications detailed below. Flag-Ddx39ab mRNA was injected into embryos from *ddx39ab* heterozygous in-crosses, with mutant embryos sorted based on GFP brightness. Deyolked embryos were homogenized in RIP buffer and briefly sonicated using the probe tip of a Branson sonicator to solubilize chromatin. Each sample was normalized for total protein amount and then Flag-Ddx39ab and associated RNA was isolated by incubation with anti-Flag agarose beads (Sigma) for 6 h at 4°C with gentle rotation. Samples were washed sequentially in high-stringency buffer, high-salt buffer and RIP buffer. Ddx39ab-associated RNA was extracted with Trizol and processed for sequencing. Sequencing libraries were prepared using the Nextera sample preparation kit and subjected to HiSeq paired-end 100 bp plus sequencing. Data analysis was performed as above.

RT-PCR analysis of splicing

Total RNA was prepared from control and *ddx39ab* mutant larvae at 36 hpf and RT-PCR performed to monitor the splicing of pre-mRNAs. Primer pairs and the PCR conditions used to amplify each of the genes are listed in Table S1.

ChIP-qPCR

Chromatin immunoprecipitation (ChIP) assays were performed as described (Lindeman et al., 2009). In brief, at 24 hpf, *ddx39ab* mutant and control embryos were collected, deyolked and cross-linked with 1% formaldehyde for 10 min at room temperature and subsequently quenched with glycine to a final concentration of 0.125 M for another 10 min. Chromatin was sonicated with a Bioruptor (Diagenode), cleared by centrifugation (10 min, 4°C, 8000 ***g***), and incubated overnight at 4°C with 5 mg anti-H3K4me1 antibody (Abcam). Immunocomplexes were immobilized with 100 µl protein-G Dynal magnetic beads (Abcam) for 4 h at 4°C, followed by stringent washes and elution. Eluates were subject to reversal of cross-links overnight at 65°C and deproteinated. DNA was extracted with phenol chloroform, followed by ethanol precipitation. H3K4me1-occupied regions at 24 hpf were retrieved from a previously reported data set (Bogdanovic et al., 2012). ChIP-qPCR analyses were performed using a Light Cycler 480II (Roche). ChIP-qPCR

signals were calculated as percentage of input. Primers used in qPCR analyses are shown in Table S1.

Acknowledgements
We thank Qi Xiao for drawing schematic pictures, Peipei Yin for zebrafish husbandry and members of the I.C.S. lab at the University of Toronto and the Di Chen lab at Nanjing University for feedback and help during this project.

Competing interests
The authors declare no competing or financial interests.

Author contributions
Conceptualization: I.C.S., X.L.; Validation: B.L.; Formal analysis: L.Z., Y.Y., B.L., X.L.; Investigation: L.Z., Y.Y., X.L.; Resources: Y.Y.; Data curation: L.Z., X.L.; Writing - original draft: X.L.; Writing - review & editing: I.C.S., X.L.; Visualization: L.Z., Y.Y., B.L.; Supervision: X.L.; Project administration: I.C.S., X.L.; Funding acquisition: I.C.S., X.L.

Funding
This research was funded, in part, by the National Natural Science Foundation of China (NSFC 31471354 and NSFC 31671505 to X.L.) and by the Natural Sciences and Engineering Research Council of Canada (RGPIN 2017-06502 to I.C.S.).

Data availability
RNA-seq data have been deposited at Gene Expression Omnibus under accession number GSE97067.

Supplementary information
Supplementary information available online at
http://dev.biologists.org/lookup/doi/10.1242/dev.161018.supplemental

References
Anders, S., Pyl, P. T. and Huber, W. (2015). HTSeq–a Python framework to work with high-throughput sequencing data. *Bioinformatics* **31**, 166-169.
Auman, H. J., Coleman, H., Riley, H. E., Olale, F., Tsai, H.-J. and Yelon, D. (2007). Functional modulation of cardiac form through regionally confined cell shape changes. *PLoS Biol.* **5**, e53.
Bassnett, S., Shi, Y. and Vrensen, G. F. J. M. (2011). Biological glass: structural determinants of eye lens transparency. *Philos. Trans. R. Soc. Lond. B Biol. Sci.* **366**, 1250-1264.
Bentzinger, C. F., Wang, Y. X. and Rudnicki, M. A. (2012). Building muscle: molecular regulation of myogenesis. *Cold Spring Harbor Perspect. Biol.* **4**, pii: a008342.
Bleichert, F. and Baserga, S. J. (2007). The long unwinding road of RNA helicases. *Mol. Cell* **27**, 339-352.
Bogdanovic, O., Fernandez-Minan, A., Tena, J. J., de la Calle-Mustienes, E., Hidalgo, C., van Kruysbergen, I., van Heeringen, S. J., Veenstra, G. J. C. and Gomez-Skarmeta, J. L. (2012). Dynamics of enhancer chromatin signatures mark the transition from pluripotency to cell specification during embryogenesis. *Genome Res.* **22**, 2043-2053.
Calo, E., Flynn, R. A., Martin, L., Spitale, R. C., Chang, H. Y. and Wysocka, J. (2015). RNA helicase DDX21 coordinates transcription and ribosomal RNA processing. *Nature* **518**, 249-253.
Clark, J. I. (2004). Order and disorder in the transparent media of the eye. *Exp. Eye Res.* **78**, 427-432.
Clark, K. J., Balciunas, D., Pogoda, H.-M., Ding, Y., Westcot, S. E., Bedell, V. M., Greenwood, T. M., Urban, M. D., Skuster, K. J., Petzold, A. M. et al. (2011). In vivo protein trapping produces a functional expression codex of the vertebrate proteome. *Nat. Methods* **8**, 506-512.
Cvekl, A. and Duncan, M. K. (2007). Genetic and epigenetic mechanisms of gene regulation during lens development. *Prog. Retin. Eye Res.* **26**, 555-597.
Ding, J.-H., Xu, X., Yang, D., Chu, P.-H., Dalton, N. D., Ye, Z., Yeakley, J. M., Cheng, H., Xiao, R.-P., Ross, J. et al. (2004). Dilated cardiomyopathy caused by tissue-specific ablation of SC35 in the heart. *EMBO J.* **23**, 885-896.
Fleckner, J., Zhang, M., Valcarcel, J. and Green, M. R. (1997). U2AF65 recruits a novel human DEAD box protein required for the U2 snRNP-branchpoint interaction. *Genes Dev.* **11**, 1864-1872.
Fuller-Pace, F. V. (2013). DEAD box RNA helicase functions in cancer. *RNA Biol.* **10**, 121-132.
Fuller-Pace, F. V. and Nicol, S. M. (2012). DEAD-box RNA helicases as transcription cofactors. *Methods Enzymol.* **511**, 347-367.
Greiling, T. M. S. and Clark, J. I. (2009). Early lens development in the zebrafish: a three-dimensional time-lapse analysis. *Dev. Dyn.* **238**, 2254-2265.
Greiling, T. M. S. and Clark, J. I. (2012). New insights into the mechanism of lens development using zebra fish. *Int. Rev. Cell Mol. Biol.* **296**, 1-61.
Gutiérrez-Aguilar, M. and Baines, C. P. (2013). Physiological and pathological roles of mitochondrial SLC25 carriers. *Biochem. J.* **454**, 371-386.
Hirabayashi, R., Hozumi, S., Higashijima, S. and Kikuchi, Y. (2013). Ddx46 is required for multi-lineage differentiation of hematopoietic stem cells in zebrafish. *Stem Cells Dev.* **22**, 2532-2542.
Hou, N., Yang, Y., Scott, I. C. and Lou, X. (2017). The Sec domain protein Scfd1 facilitates trafficking of ECM components during chondrogenesis. *Dev. Biol.* **421**, 8-15.
Hozumi, S., Hirabayashi, R., Yoshizawa, A., Ogata, M., Ishitani, T., Tsutsumi, M., Kuroiwa, A., Itoh, M. and Kikuchi, Y. (2012). DEAD-box protein Ddx46 is required for the development of the digestive organs and brain in zebrafish. *PLoS ONE* **7**, e33675.
Huang, D. W., Sherman, B. T. and Lempicki, R. A. (2009). Systematic and integrative analysis of large gene lists using DAVID bioinformatics resources. *Nat. Protoc.* **4**, 44-57.
Huang, W., Thomas, B., Flynn, R. A., Gavzy, S. J., Wu, L., Kim, S. V., Hall, J. A., Miraldi, E. R., Ng, C. P., Rigo, F. et al. (2015). DDX5 and its associated lncRNA Rmrp modulate TH17 cell effector functions. *Nature* **528**, 517-522.
Jain, R., Devine, T., George, A. D., Chittur, S. V., Baroni, T. E., Penalva, L. O. and Tenenbaum, S. A. (2011). RIP-Chip analysis: RNA-binding protein immunoprecipitation-microarray (Chip) profiling. *Methods Mol. Biol.* **703**, 247-263.
Jarmoskaite, I. and Russell, R. (2011). DEAD-box proteins as RNA helicases and chaperones. *Wiley Interdiscip. Rev. RNA* **2**, 135-152.
Jarmoskaite, I. and Russell, R. (2014). RNA helicase proteins as chaperones and remodelers. *Annu. Rev. Biochem.* **83**, 697-725.
Kawakami, K., Asakawa, K., Muto, A. and Wada, H. (2016). Tol2-mediated transgenesis, gene trapping, enhancer trapping, and Gal4-UAS system. *Methods Cell Biol.* **135**, 19-37.
Kim, D., Pertea, G., Trapnell, C., Pimentel, H., Kelley, R. and Salzberg, S. L. (2013). TopHat2: accurate alignment of transcriptomes in the presence of insertions, deletions and gene fusions. *Genome Biol.* **14**, R36.
Langmead, B. and Salzberg, S. L. (2012). Fast gapped-read alignment with Bowtie 2. *Nat. Methods* **9**, 357-359.
Lee, J.-E., Wang, C., Xu, S., Cho, Y.-W., Wang, L., Feng, X., Baldridge, A., Sartorelli, V., Zhuang, L., Peng, W. et al. (2013). H3K4 mono- and di-methyltransferase MLL4 is required for enhancer activation during cell differentiation. *eLife* **2**, e01503.
Lindeman, L. C., Vogt-Kielland, L. T., Aleström, P. and Collas, P. (2009). Fish'n ChIPs: chromatin immunoprecipitation in the zebrafish embryo. *Methods Mol. Biol.* **567**, 75-86.
Linder, P. and Jankowsky, E. (2011). From unwinding to clamping - the DEAD box RNA helicase family. *Nat. Rev. Mol. Cell Biol.* **12**, 505-516.
Luo, M.-J., Zhou, Z., Magni, K., Christoforides, C., Rappsilber, J., Mann, M. and Reed, R. (2001). Pre-mRNA splicing and mRNA export linked by direct interactions between UAP56 and Aly. *Nature* **413**, 644-647.
Meignin, C. and Davis, I. (2008). UAP56 RNA helicase is required for axis specification and cytoplasmic mRNA localization in Drosophila. *Dev. Biol.* **315**, 89-98.
Payne, E. M., Bolli, N., Rhodes, J., Abdel-Wahab, O. I., Levine, R., Hedvat, C. V., Stone, R., Khanna-Gupta, A., Sun, H., Kanki, J. P. et al. (2011). Ddx18 is essential for cell-cycle progression in zebrafish hematopoietic cells and is mutated in human AML. *Blood* **118**, 903-915.
Pillai-Kastoori, L., Wen, W. and Morris, A. C. (2015). Keeping an eye on SOXC proteins. *Dev. Dyn.* **244**, 367-376.
Rao, R. C. and Dou, Y. (2015). Hijacked in cancer: the KMT2 (MLL) family of methyltransferases. *Nat. Rev. Cancer* **15**, 334-346.
Ríos, Y., Melmed, S., Lin, S. and Liu, N.-A. (2011). Zebrafish usp39 mutation leads to rb1 mRNA splicing defect and pituitary lineage expansion. *PLoS Genet.* **7**, e1001271.
Rocak, S. and Linder, P. (2004). DEAD-box proteins: the driving forces behind RNA metabolism. *Nat. Rev. Mol. Cell Biol.* **5**, 232-241.
Rösel, T. D., Hung, L.-H., Medenbach, J., Donde, K., Starke, S., Benes, V., Rätsch, G. and Bindereif, A. (2011). RNA-Seq analysis in mutant zebrafish reveals role of U1C protein in alternative splicing regulation. *EMBO J.* **30**, 1965-1976.
Sarkar, M. and Ghosh, M. K. (2016). DEAD box RNA helicases crucial regulators of gene expression and oncogenesis. *Front. Biosci.* **21**, 225-250.
Schmittgen, T. D. and Livak, K. J. (2008). Analyzing real-time PCR data by the comparative C(T) method. *Nat. Protoc.* **3**, 1101-1108.
Sheets, K. G., Jun, B., Zhou, Y., Winkler, J., Zhu, M., Petasis, N., Gordon, W. C. and Bazan, N. G. (2011). Topical neuroprotectin D1 attenuates experimental CNV and induces activated microglia redistribution. *Invest. Ophthalmol. Vis. Sci.* **52**, 5470-5470.
Shen, J., Zhang, L. and Zhao, R. (2007). Biochemical characterization of the ATPase and helicase activity of UAP56, an essential pre-mRNA splicing and mRNA export factor. *J. Biol. Chem.* **282**, 22544-22550.
Shen, H., Zheng, X., Shen, J., Zhang, L., Zhao, R. and Green, M. R. (2008). Distinct activities of the DExD/H-box splicing factor hUAP56 facilitate stepwise assembly of the spliceosome. *Genes Dev.* **22**, 1796-1803.

Sugiura, T., Sakurai, K. and Nagano, Y. (2007). Intracellular characterization of DDX39, a novel growth-associated RNA helicase. *Exp. Cell Res.* **313**, 782-790.
Thisse, C. and Thisse, B. (2008). High-resolution in situ hybridization to whole-mount zebrafish embryos. *Nat. Protoc.* **3**, 59-69.
Walter, W., Sánchez-Cabo, F. and Ricote, M. (2015). GOplot: an R package for visually combining expression data with functional analysis. *Bioinformatics* **31**, 2912-2914.
Westerfield, M. (1993). *The Zebrafish Book: A Guide for the Laboratory Use of Zebrafish Danio (Brachydanio) rerio*. Eugene, Oregon: University of Oregon Press.
Wu, J., Anczuków, O., Krainer, A. R., Zhang, M. Q. and Zhang, C. (2013). OLego: fast and sensitive mapping of spliced mRNA-Seq reads using small seeds. *Nucleic Acids Res.* **41**, 5149-5163.
Xu, X., Yang, D., Ding, J.-H., Wang, W., Chu, P.-H., Dalton, N. D., Wang, H.-Y., Bermingham, J. R., Jr, Ye, Z., Liu, F. et al. (2005). ASF/SF2-regulated CaMKIIdelta alternative splicing temporally reprograms excitation-contraction coupling in cardiac muscle. *Cell* **120**, 59-72.
Yazaki, P. J., Salvatori, S., Sabbadini, R. A. and Dahms, A. S. (1990). Calsequestrin, an intracellular calcium-binding protein of skeletal muscle sarcoplasmic reticulum, is homologous to aspartactin, a putative laminin-binding protein of the extracellular matrix. *Biochem. Biophys. Res. Commun.* **166**, 898-903.
Yoo, H. H. and Chung, I. K. (2011). Requirement of DDX39 DEAD box RNA helicase for genome integrity and telomere protection. *Aging Cell* **10**, 557-571.
Zhang, F., Wang, J., Xu, J., Zhang, Z., Koppetsch, B. S., Schultz, N., Vreven, T., Meignin, C., Davis, I., Zamore, P. D. et al. (2012). UAP56 couples piRNA clusters to the perinuclear transposon silencing machinery. *Cell* **151**, 871-884.

Supplementary material

Table S1. Primers sequences and PCR conditions.

Click here to Download Table S1

Table S2. List of antibodies used for western, CHIP, RIP and immunofluorescence studies.

Antibody name	Company	Dilution	Application
Anti-α tubulin	Santa Cruz Biotechnology (sc-23948)	1:2000	Western blotting
Anti-Nkx2.5	Cell Signaling Technology (8792)	1:1000	Western blotting
Anti-Gata4	Santa Cruz Biotechnology (sc-25310)	1:1000	Western blotting
Anti-Myf5	GeneTex (GTX87746)	1:1000	Western blotting
Anti-MyoD	Santa Cruz Biotechnology (sc-377460)	1:500	Western blotting
Anti-Mef2C	Cell Signaling Technology (5030)	1:1000	Western blotting
Anti-Histone 3	Cell Signaling Technology (9715)	1:1000	Western blotting
Anti-H3K4Me1	Abcam (ab8895)	1:500	Western blotting
		2 µg for 25 µg of chromatin	CHIP
Anti-Actin	SIGMA (A2172)	1:200	Immunostaining
Anti-Myosin	DSHB (MF20)	1:200	Immunostaining
ANTI-FLAG M2 Affinity Gel	SIGMA (A2220)	N.A	RIP
Anti-MYH1A	DSHB (F59)	1:50	Immunostaining
Anti-CD166	DSHB (zn8)	1:50	Immunostaining
Anti-TNNT2	Santa Cruz Biotechnology (sc-20025)	1:50	Immunostaining
Anti-mouse IgG (H+L),-Alexa Fluor 594 Conjugate	Cell Signaling Technology (8890)	1:200	Immunostaining
Anti-Rabbit IgG (H+L)-Alexa Fluor 568 Conjugate	Thermo Fisher (A10042)	1:200	Immunostaining

Development • Supplementary information

Table S3. Significant different expression gene in *ddx39ab* mutant. This file includes Genes that that have FDR≤0.001 and Fold Change >2.

Click here to Download Table S3

Table S4. Significant alternative splicing events in *ddx39ab* mutant embryo. Four types of alternative splicing events, including exon skipping, intron retention, 5' and 3' splicing sites usage, were calculated from the RNA-seq data of control and *ddx39ab* mutant embryo (24hpf) by the OLego and Quantas software packages. The spread sheet for each type of events contains 7 columns, including gene accession number, chromosome, strand, constitutive exon, alternative events.

Click here to Download Table S4

Table S5. Gene Ontology (GO) enrichment analysis of significant different expression gene in *ddx39ab* mutant. P<0.01, FDR<0.05.

Click here to Download Table S5

Table S6. List of Ddx39ab-interacting RNAs identified by RIP-Seq analysis. q value≤0.1.

Click here to Download Table S6

Development • Supplementary information

Movie 1. Contraction of the definitive heart tube in RP -011 homozygous and control embryo.

Movie 2. Spontaneous tail movements in RP -011 homozygous and control embryo.

Development • Supplementary information

Supplementary figures

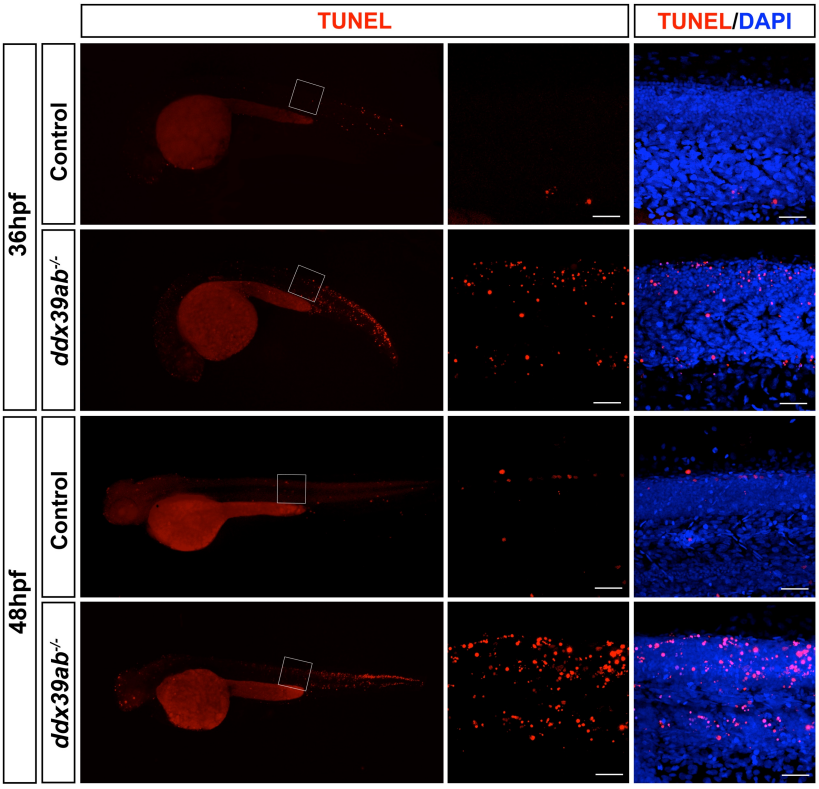

Supplemental Figure 1. **Cell death in wild type or *ddx39ab* mutant embryo.** Right panels, magnified view of the boxed region. Scale bars, 20um. For each stage, at least 10 embryos for each genotype were analyzed and representative samples are shown.

Development • Supplementary information

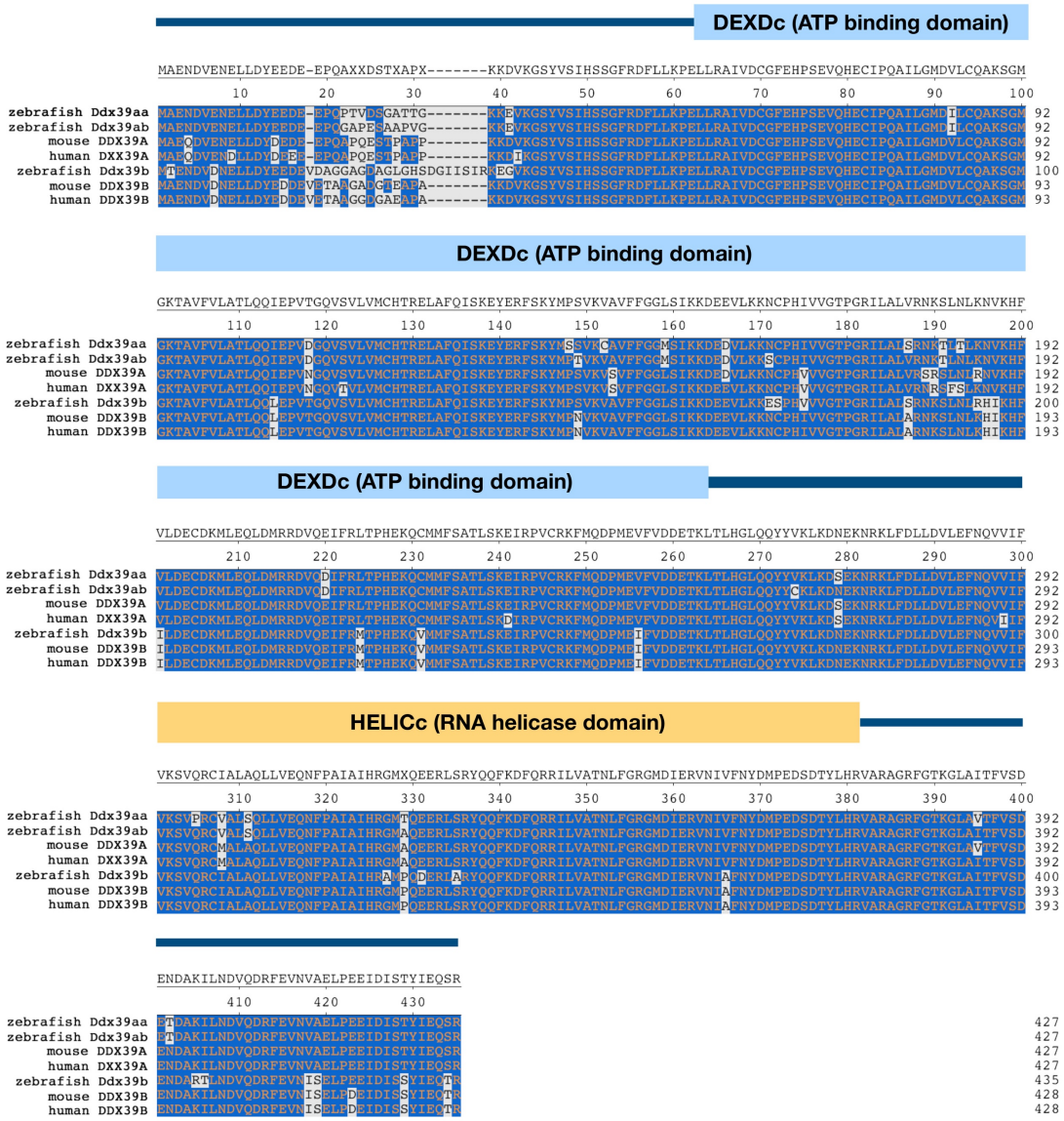

Supplemental Figure 2. DDX39 protein sequences alignment. Functional domains are labeled. The orthologs and paralogs of DDX39 in zebrafish, mouse and human share 94% amino acid identity, differing in only 21 residues.

Development • Supplementary information

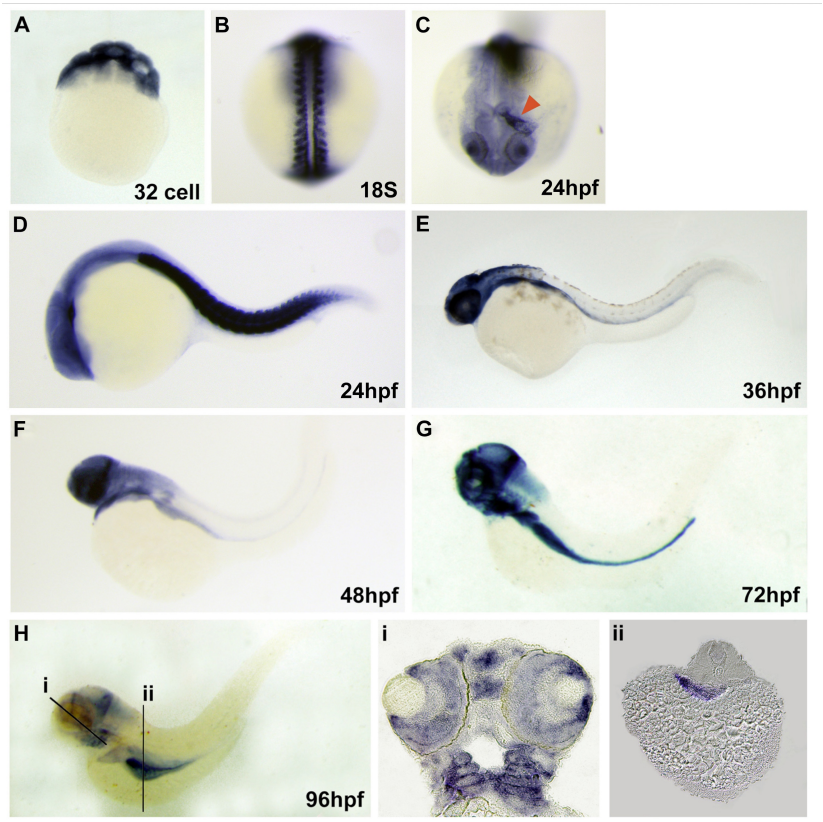

Supplemental Figure 3. Zebrafish *ddx39ab* embryonic expression pattern. (A): In situ hybridization experiment revealed there is maternal deposit ddx39ab mRNA in early stage embryo. (B): Strong expression of *ddx39ab* could be observed in myotome at 18 somite stage. (C-D): At 24hpf enriched *ddx39ab* mRNA could be observed in lens, heart tube and trunk muscle. Triangle indicated expression in heart tube. (E-H): Later on, the expression was restrained to specific regions in brain, retina (i), pharyngeal arches (i) and endoderm derived organs (ii). A, lateral view. B, dorsal view. C, frontal view. D to H, head to left. i and ii are sections of H as indicated. hpf, hour past fertilization.

Development • Supplementary information

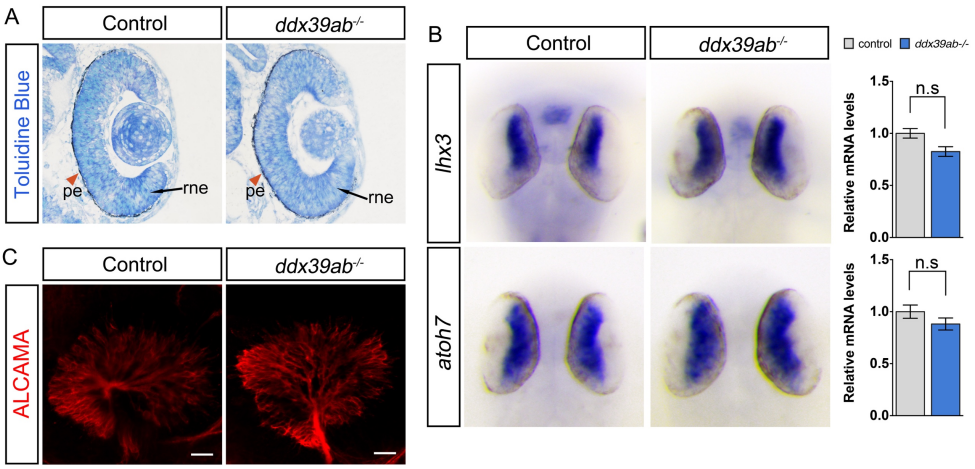

Supplemental Figure 4. Retina development in *ddx39ab* mutants. (A): Frontal sections of retina at 32 hpf. (B): RNA *in situ* hybridization and qPCR results are shown for retinal ganglion marker gene expression in control and *ddx39a* mutant zebrafish embryos. Dorsal views with anterior to the top. For qPCR results, data are mean ± SEM. ns: not significant. (C): Confocal images of retinal ganglion cell (labeled with zn8 antibody) from wild type and *ddx39ab* mutant embryo at 48 hpf. Scale bars, 20um. A, B and C, at least 15 embryos for each genotype were analyzed and representative samples are shown.

Development • Supplementary information

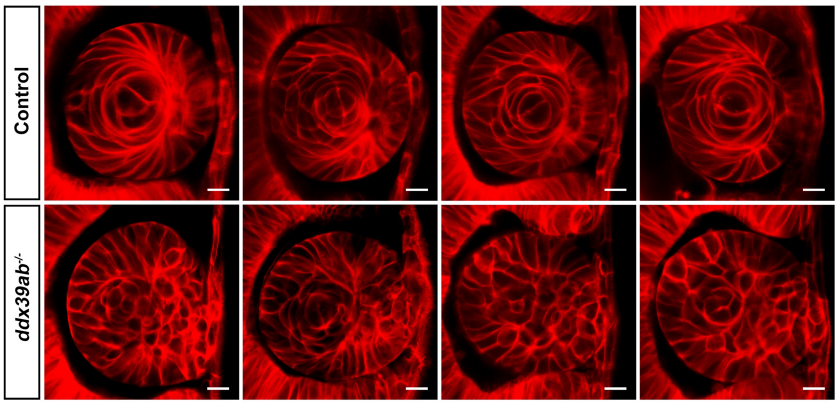

Supplemental Figure 5. Disorganization of primary lens fiber cell in *ddx39a* embryo. Cell membrane was labeled with mRFP; living images were taken at 28 hpf. Scale bars, 25 μM.

Development • Supplementary information

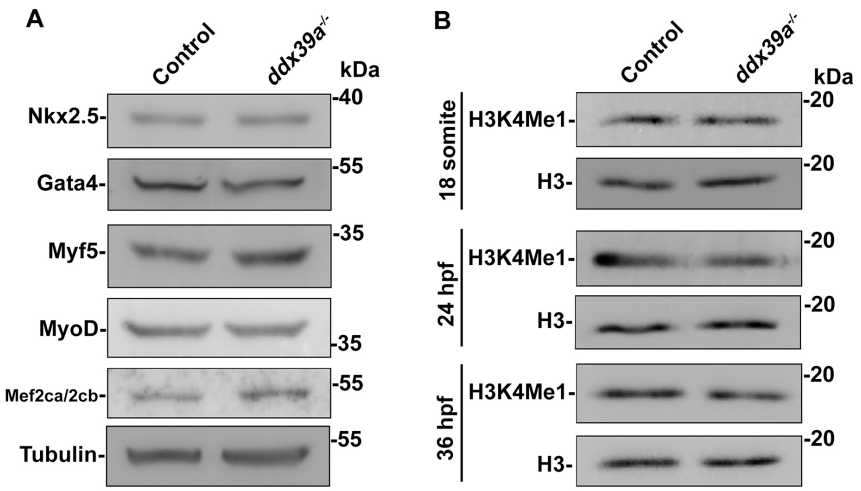

Supplemental Figure 6. Western blot analysis of the indicated proteins and histone PTMs in control and *ddx39ab* mutant embryo. (A): protein level of myocyte or cardiomyocyte key transcription regulators showed no evident change between control and *ddx39a* mutant at 24 hpf. (B): In *ddx39ab* mutant, minor decrease on H3K4Me1 level could be detected from 24 hpf.

Development • Supplementary information

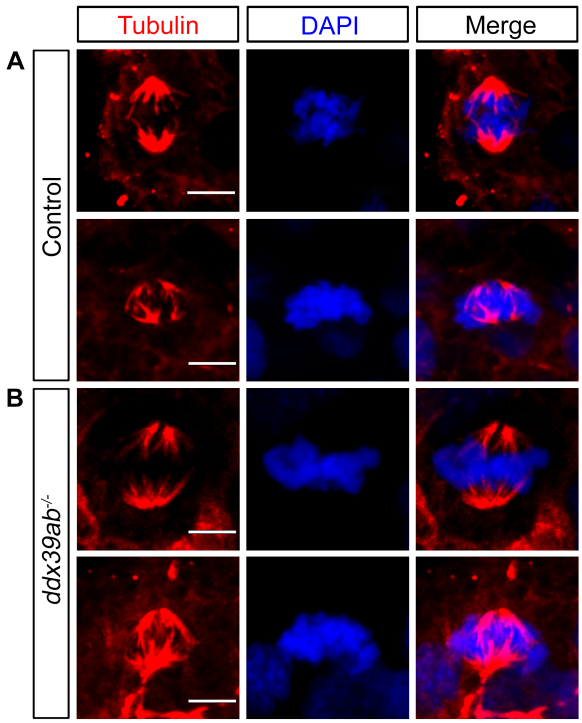

Supplemental Figure 7. *Ddx39ab* mutant embryos exhibit normal mitoses. Mitotic cells stained with DAPI (blue) and α-tubulin (red). Scale bars, 5um.

Development • Supplementary information

Supplementary Materials and Methods

Western blotting

Proteins were isolated by homogenizing embryos in RIPA buffer containing protease inhibitor (Sigma). Proteins were separated by sodium dodecyl sulfate-polyacrylamide gel electrophoresis (SDS-PAGE). For immunoblotting, proteins were transferred to polyvinylidene fluoride (PVDF) membrane using an electrophoretic transfer apparatus (Bio-Rad). The membrane was blocked with 1% non-fat milk (Bio-Rad) and incubated with primary antibody followed by 1:10,000 HRP-conjugated secondary antibodies (Sigma). Signal detection was performed using Pico West Chemiluminescent Substrate (Thermo Scientific). Information for primary antibodies are listed in Supplementary Table 2.

Development • Supplementary information